

Influence of p16 Protein Immunostaining on Histopathological Features of Pleomorphic Adenoma and Carcinoma ex- Pleomorphic Adenoma

Iana Aragao Magalhaes¹, Kecynara Costa Barbosa¹, Gabriela Alves Juliao Costa^{1,2}, Osias Vieira de Oliveira Filho¹, Jose Erialdo da Silva Junior², Lucio Flavio Gonzaga e Silva², Sergio Ferreira Juacaba², Fabricio Bitu Sousa¹, Paulo Goberlanio de Barros Silva^{1,2*}

Abstract

The objective of this study was to evaluate the role of p16 in histologic characteristics and transition of Pleomorphic Adenoma (PA) to Carcinoma ex-PA (CxPA). So, 60 PA and 4 CxPA were histologic reviewed based on microscopic characteristics proposed by Hellquist, Triantafyllou and Dulguerov (PA) and Morais, Antony and Toluie (CxPA). Immunostaining for p16 was associated in different parenchyma and stroma of both tumors and Fisher's/chi-square tests and Mann-Whitney test were performed (SPSS v20.0, $p < 0.05$). In PA the periductal cells were predominantly p16- and that ductal and myoepithelial cells showed a significant increase in p16+ cells ($p < 0.001$). In CxPA, none of the cases showed p16+ in periductal cells, most parotid cases showed p16+ in ductal cells, and one case of parotid and the submandibular case showed mild immunostaining for myoepithelial cells. There was a small reduction in p16+ in CxPA compared to PA ($p = 0.537$), but in both tumors there was less p16+ cells in solid stroma than other ($p < 0.001$). The p16+ cases of PA had a higher capsular thickness ($p = 0.047$). So, the loss of p16 immunostaining does not seem to be associated with the transition from PA to CxPA, but in both tumors the loss of p16+ cells are related to microscopic aggressiveness.

Keywords: Adenoma- pleomorphic- salivary gland neoplasms- genes- p16

Asian Pac J Cancer Prev, 24 (11), 3815-3824

Introduction

Pleomorphic adenoma (PA) consists of a benign salivary gland neoplasm, which arises due to the architectural pleomorphism, morphological complexity, and diversity in the tumor (Choi et al., 2019). Among the benign salivary gland tumors, Warthin tumor, myoepithelioma, and oncocytoma, PA is the most common tumor, corresponding to 91.3% of cases. Moreover, it is considered the most common neoplasm of all benign and malignant salivary tumors, accounting for 59.6% of the total (Reinheimer et al., 2019).

PA has been reported in young, young adults, and middle-aged adults, occurring most frequently in adult women between the third and fifth decade of life. Salivary gland tumors are rare in children, mainly in the minor salivary glands; however, PA is the most common benign tumor in children and parotid (Ahmedi et al., 2017).

The PA presents clinically as a volume increase with a slow progression, asymptomatic, with location

most commonly in the parotid gland region, without the involvement of the facial nerve (Sergi et al., 2008). They are usually discovered during a routine physical examination, measuring about 2 to 5 cm. The smaller diameter tumors have firm and mobile palpation. In contrast, those of larger diameter may have protrusions that attenuate the overlying skin or mucosa (Thompson, 2006). Although PA manifests mainly in parotid glands, another preferred location is the palate. In addition to the palate, other intraoral affected sites are the upper lip, buccal mucosa, tongue, and gingiva (Erdem et al., 2011).

Histologically, PAs have an epithelial component, a myoepithelial cell component, a mesenchymal component (Almeslet, 2020), and has connective tissue capsule that may be incomplete (Ahmedi et al., 2017). In the epithelial region, tubular or solid structures contain luminal epithelial cells in the inner layer, and the non-luminal myoepithelial cells in the outer layer (Lee et al., 2000) dispersed in the mesenchyme of the lesion (Batsakis et al., 1983). The main cells that make up PA are myoepithelial cells, which

¹Unichristus, Department of Dentistry, Fortaleza, Ceará, Brazil. ²Haroldo Juaçaba Hospital, Ceará Cancer Institute, Fortaleza, Ceará, Brazil. *For Correspondence: paulo_goberlanio@yahoo.com.br

have a morphological diversity due to their considerable degree of cytological modification. The spectrum of cytological transformation consists of the appearance of fusiform, transparent, cuboidal or plasmacytoid cells. The mesenchymal region of the tumor is formed by a variable fibromyxoid chondroid area. According to Lee and co-workers, in the PA tissues examined in their study, the epithelial and mesenchymal elements arise from the same cell clone, which may be a myoepithelial or ductal cell (Batsakis et al, 1983; Dardick and van Nostrand, 1985).

It is important to stress that PAs should have diligent treatment because of the tendency to recur and malignant transformation, which consists of change into carcinoma ex-PA (CxPA) (Jain et al., 2015). CxAP is a carcinoma arising from primary (de novo) or recurrent benign PA12. According to Andreasen and colleagues, the frequency of malignant transformation in patients with recurrent PA was 3.3% as opposed to 0.25% in patients with primary PA alone. Therefore, among the risk factors, it is essential to consider in the clinical evaluation the following characteristics facing the possibility of malignant transformation: age, tumors located in minor salivary glands, being the main sites of involvement of carcinoma ex- PA, and enlargement of regional lymph nodes (Seok et al., 2019; Andreasen et al., 2016).

The p16 protein encoded by the INK4a gene located on chromosome 9p21 acts as a negative regulator of the cell cycle, one of the primary mechanisms for preventing tumor formation (Romagosa et al., 2011). The function of p16 consists in the inhibition of cyclin-dependent kinase 4 (CDK4), which prevents the formation of the CDK4/Cyclin D complex, resulting in the inhibition of the phosphorylation of the retinoblastoma susceptibility protein (pRB) (Serrano et al., 1993). According to the author Jour, the p16 protein was expressed in benign and malignant salivary gland tumors, including the PA and CxPA. Furthermore, in benign tumors that express positive staining of p16, this protein demonstrates the ability to protect the cell from malignant transformation due to the control of the proliferation of oncogenic stimuli (Romagosa et al., 2011; Serrano et al., 1993; Jour et al., 2013).

Moreover, through immunohistochemistry with p16 antibody, one can detect relevant associations between HPV infection and the development of head and neck tumors since several articles prove that HPV is involved in the pathogenesis of squamous cell carcinoma (SCC). The literature describes a possible involvement of HPV in the oncogenesis of salivary gland tumors (Vageli et al., 2007).

So, as a better understanding of p16 overexpression in PA and CxPA will contribute to understanding the biological behavior of the cellular elements of these two such heterogeneous stromal tumors, the objective of this study was to evaluate the role of p16 immunostaining in histologic characteristics and transition of PA to CxPA.

Materials and Methods

Study type and patient samples

This is a quantitative and cross-sectional study. The biological samples of PA and CxPA were collected through

a survey of clinical-pathological data of patients who underwent surgery for resection of salivary gland cancers at the Hospital Haroldo Juaçaba/Instituto do Câncer do Ceará (HHJ/ICC), between 2010 and 2020. We excluded specimens with incomplete clinicopathological data that did not have sufficient amounts of biological material to perform immunohistochemistry, slides and blocks damaged or deficient for microscopy, and tumors from patients who underwent neoadjuvant treatment.

After selecting the collected specimens based on the inclusion and exclusion criteria, the study counted 60 samples of PAs and four samples of carcinomas ex-PA fixed in formalin and embedded in paraffin from tissues removed by excisional biopsy, in which they were submitted to histopathological review by a pathologist with more than ten years of experience to confirm the diagnosis of the tumors.

The tumors were divided into two study groups, a group consisting of 60 PAs and a group composed of 04 carcinomas ex PA; each group was subjected to histomorphological and immunohistochemical analysis for p16, and the expression of the protein in the stromal patterns of each group was compared.

Immunohistochemical processing

Paraffin blocks containing the tumor tissue samples were sectioned to a thickness of 4 µm and mounted on silanized glass slides. Then, the sections were deparaffinized with xylene and rehydrated in graded concentrations of alcohol. Immediately after, antigen retrieval was performed by incubating the slide in Tris-EDTA solution under the temperature of 98°C for 20 minutes in the PTLINK® system (Dako®). Then the slides were cooled at room temperature for 20 minutes and washed with phosphate-buffered saline (PBS) solution.

Subsequently, endogenous peroxidase was blocked with 3% hydrogen peroxide diluted in buffer solution for 30 minutes, followed by further washes with buffer solution and overnight incubation with the primary mouse monoclonal antibody, clone D25 (Merck®), directed against the p16 protein.

After the incubation period with the primary antibody, the slides were washed with PBS and incubated with the Envision system (Dako®) for 30 minutes. Then, the slides were washed with PBS for 10 minutes and incubated with a solution prepared with DAB chromogenic reagent (3,3' - diaminobenzidine-tetrachloride) for 5 minutes for development. Finally, counterstaining of the slides with Harris hematoxylin for 10 seconds, dehydration in ethanol, clarification in xylene, and mounting for analysis were performed.

A p16+ oropharyngeal carcinoma sample was used as a positive control for the immunohistochemistry reaction. The same immunohistochemistry technique described above was used as a negative control but omitted the primary antibody's incubation step.

Histomorphology analysis of PA

PA slides were evaluated according to the criteria previously published:

The criteria by Hellquist et al., (2019) included:

- Presence of Oncocytic, Bone, Sebaceous, Lipomatous, or Squamous metaplasias
- Predominant cellular pattern: classified as nodular/multinodular or luminal/non-luminal cells
- Other features: presence of crystalloids, pigmentation, nerves, or blood vessels within tumor.

The criteria by Triantafyllou et al., (2015) included:

- Squamous metaplasias: when present, they were categorized to the extent as up to 50% of the tumor, more than 50%, and with keratin pearl formation;
- Predominant stromal pattern: myxoid, chondroid, hyaline, bony, or adipocytic
- Separation between cells and stroma: categorized by demarcated or indistinct.

The criteria by Dulguerov et al., (2017) included:

- Capsular invasion and average capsule thickness: when present, the most significant depth was assessed.
- Predominant cellular pattern: classified as hypocellular, classical or hypercellular.
- Other features: presence of pseudopodia or satellite nodules, compromised surgical margin, and intentional or unintentional rupture of the capsule.

Histomorphology analysis of CxPA

CxPA slides were evaluated considering these criteria previously published:

The criteria by Morais et al., (2019) included

- Presence of extracapsular invasion;

The criteria by Antony et al., (2012) included:

- Dominant cell profile: luminal or non-luminal cell;
- Cellular features: presence of nuclear pleomorphism, mitosis figures, atypical mitoses, hemorrhage, necrosis, or association with another salivary gland tumor.

The criteria by Toluie et al., (2012) included:

- Prognostic features: presence of perineural invasion, angiolymphatic invasion, bone invasion, nodal metastasis, and higher nucleus-cytoplasm ratio.

Immunohistochemical Analysis

The p16 protein expression pattern was classified according to the percentage of immunopositive cells in the different stromal patterns of the samples by two blinded researchers and mean of positivity was the sample unity. The cells with brown pigmentation observed within the nucleus and/or cytoplasm were considered positive. The value of the intraclass correlation coefficient was 0.922.

Statistical Analysis

The data were tabulated in a standard Microsoft Excel spreadsheet and exported to SPSS v20.0 software, in which the analyses were performed adopting a 95% confidence level. Clinical data and pathological characteristics were expressed as absolute and percentage frequency and morphometry data and rate of p16+ cells as mean and standard deviation. The percentage of p16+ cells was categorized based on the median, and the categories were associated with other characteristics

employing Fisher's exact test or Pearson's chi-square and Mann-Whitney tests.

Ethical Aspects

This research was submitted to the Research Ethics Committee of the HHJ/ICC, observing the norms that regulate research with human beings, of the National Health Council under resolution 466/12. The opinion number was 2.251.564.

Results

Characterization of the sample: PA

Our sample consisted of 60 PAs and 04 carcinomas ex PAs. Of the 60 PAs, most cases (n=37, 61.7%) were female. The mean age of the patients was 45.5±16.6, with the youngest patient being 19 years old and the oldest being 87 years old. Half of the sample was up to 45 years old. The most frequent location was in the parotid gland, affecting 47 patients (81.0%) (Table 1).

Regarding the parameters proposed by Hellquist et al., (2019), multifocal tumors were seen only in 3 cases (5.3%), and most cases were focal tumors. The most frequently found metaplasia was squamous metaplasia present in 28 patients (46.6%), followed by oncocytic metaplasia seen in 22 patients (36.7%); bony and sebaceous metaplasias were not seen in any case. Among the 28 patients with squamous metaplasia, 23 had this metaplasia in up to 50% of the sample, and 5 had keratin poles. The capsular invasion occurred in 10 cases (16.7%) with a mean depth of 694.44±680.28 µm (Table 1).

Whereas in the histological parameters proposed by Triantafyllou et al., (2015), most cases were multinodular (n= 35, 58.3 %), the predominant cells were non-luminal cells (n=51, 85.0%), myxoid stroma was the most frequent, seen in 95.0% of cases, followed by hyaline/fibrous stroma present in 50.0%, chondroid present in 41.7%. Adipocytic stroma was seen in only 9 cases (15.0%), and bone stroma was seen in none. The separation between cells and stroma was well limited in most cases, with 85.0% being well demarcated. Additionally, crystalloids were observed only in 3 cases (5.0%), microliths in none, pigmentation in 4 (6.7%), vessels and nerves in 24 (40.0%), and 7 (11.7%), respectively. The mean capsule thickness was 95.68±75.03 µm (Table 1).

Regarding the parameters of Dulguerov et al., (2017), no patient showed facial nerve involvement. The dominant stroma was myxoid (n=50, 93.3%), followed by chondroid with 4 cases (6.7%), and mucous, fibrous and sparse showed only 2 cases each (3.3%). The predominant cellular profile was the classic or balanced profile (30-50% stroma) with 22 cases (36.7%), followed by the hypercellular profile (<30% stroma) with 20 cases (33.3%) and the hypocellular profile with 18 cases (30.0%). Pseudoploidy was observed in only three cases (5.0%) and satellite nodules in two (3.3%). Surgical margins were free in most cases (n= 52, 88.1%), and the surgical margin distance was 0.91±0.46 cm. Puncture tumor and spillage were not observed in any of the cases. The mean capsular integrity was 95.17±12.28%. The minimum capsular thickness was 39.83±33.81 µm, and the maximum capsular thickness

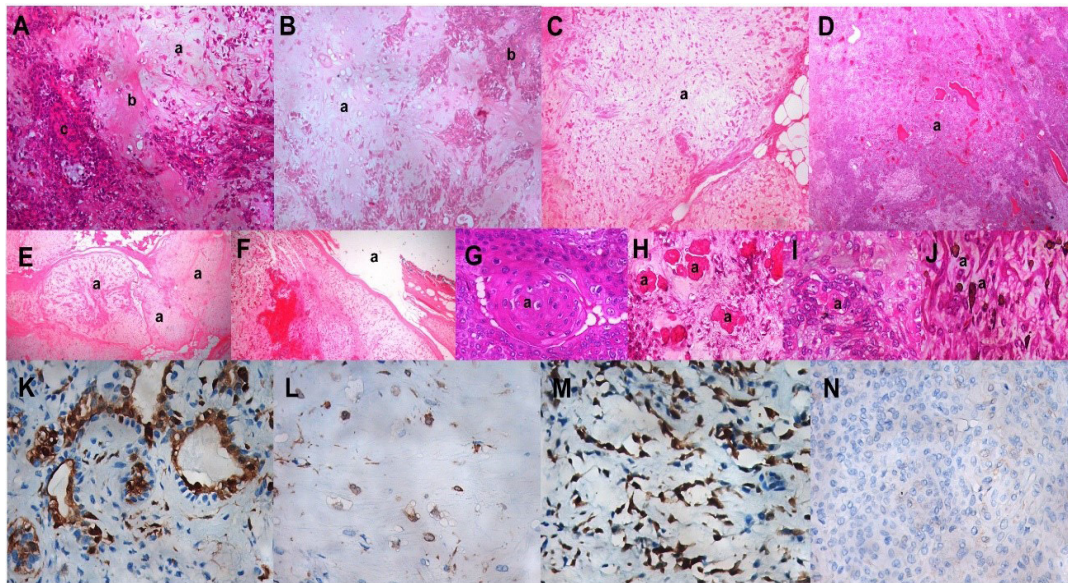


Figure 1. Histological Features and Immunostaining for p16 in PA. A: classic pattern pleomorphic adenoma showing myxoid (a), hyaline (b) and solid (c) stroma; B: classic pattern pleomorphic adenoma showing chondroid (a) and solid (b) stroma; C: hypocellular pattern pleomorphic adenoma showing predominantly myxoid stroma (a); D: hypercellular pattern pleomorphic adenoma showing predominantly solid stroma (a); E: Hypocellular pattern pleomorphic adenoma showing multinodular distribution (a); F: hypocellular pattern pleomorphic adenoma showing partial capsule rupture (a); G: keratin pearl-shaped squamous metaplasia (a); H: crystalloids (a); I: oocytic metaplasia; J: pigmentations (a); K: positive immunostaining for p16 in luminal ductal cells, and negative in non-luminal ductal cells; L: positive immunostaining for p16 in chondroid stroma; M: positive immunostaining for p16 in myxoid stroma (myoepithelial cells); N: negative immunostaining for p16 in solid stroma.

was 311.00 ± 271.73 micrometers. The maximum tumor size was 2.70 ± 1.19 cm (Table 1).

The mean and median percentage of immunostaining for p16 in the PAs was $11.35 \pm 13.93\%$ and 5% ,

respectively, ranging from 0-50%. The profile for p16 protein was very variable, sometimes marking ductal, periductal, and sometimes myoepithelial cells. In most cases, periductal cells were negative for p16, whereas

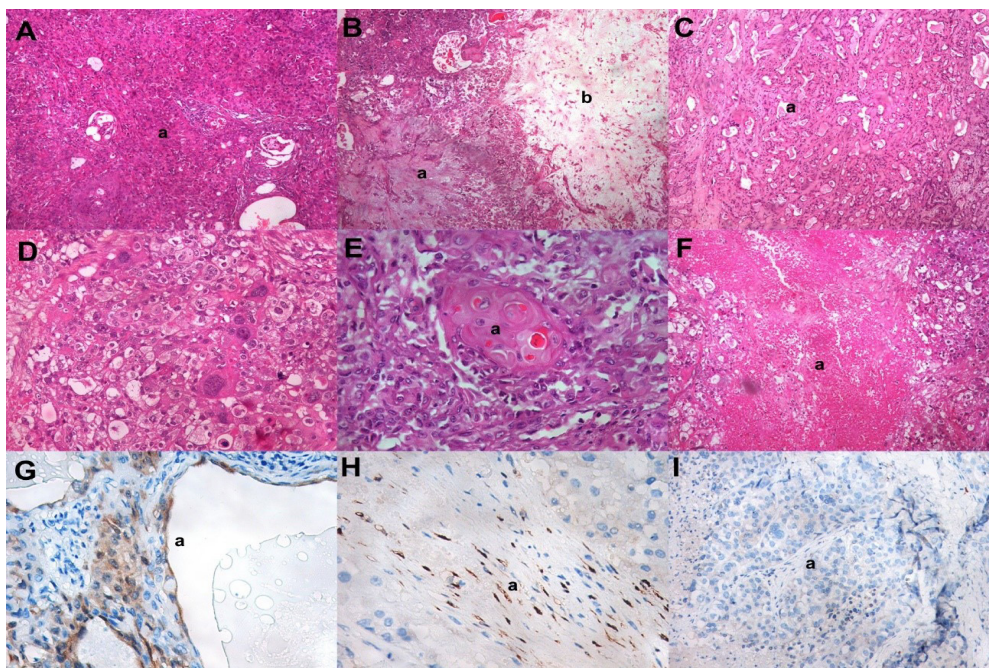


Figure 2. Histological Features and Immunostaining for p16 in CxPA. A: carcinoma ex pleomorphic adenoma hypercellular pattern showing solid stroma (a); B: carcinoma ex pleomorphic adenoma hypercellular pattern showing hyaline (a) and myxoid (b) stroma; C: classical pattern pleomorphic carcinoma ex-adenoma showing large amounts of ductal cells (a); D: carcinoma ex-pleomorphic adenoma showing extensive cellular and nuclear pleomorphism; E: carcinoma ex-pleomorphic adenoma showing keratin pearl (a); F: carcinoma ex-pleomorphic adenoma showing large areas of intratumoral hemorrhage (a); G: positive immunostaining for p16 in luminal ductal cells, and negative in non-luminal ductal cells; H: positive immunostaining for p16 in myxoid stroma (myoepithelial cells); I: negative immunostaining for p16 in solid stroma.

Table 1. Influence of p16 Immunostaining on the Clinicopathological Profile of PAs

	Total	p16 (%)		p- value
		Up to 5%	>5%	
Total	60	33 (55.0%)	27 (45.0%)	-
Sex				
Female	37 (61.7%)	23 (69.7%)	14 (51.9%)	0.157 ^a
Male	23 (38.3%)	10 (30.3%)	13 (48.1%)	
Location				
Parotid	47 (81.0%)	26 (78.8%)	21 (84.0%)	0.742 ^a
Submandibular	11 (19.0%)	7 (21.2%)	4 (16.0%)	
Age				
Up to 45	30 (50.0%)	16 (48.5%)	14 (51.9%)	0.795 ^a
>45	30 (50.0%)	17 (51.5%)	13 (48.1%)	
Hellquist (18) parameters				
Multifocal tumor	3 (5.3%)	2 (6.3%)	1 (4.0%)	1.000 ^a
Metaplasia				
Oncocytic	22 (36.7%)	15 (45.5%)	7 (25.9%)	0.118 ^a
Lipomatous	4 (6.7%)	2 (6.1%)	2 (7.4%)	1.000 ^a
Squamous metaplasia				
No	32 (53.3%)	16 (48.5%)	16 (59.3%)	0.448 ^a
Up to 50	23 (38.3%)	13 (39.4%)	10 (37.0%)	
Keratin Pearls	5 (8.3%)	4 (12.1%)	1 (3.7%)	
Capsular invasion	10 (16.7%)	7 (21.2%)	3 (11.1%)	0.488 ^a
Invasion depth (µm)	694.44±680.28	464.29±582.18	1500	0.073 ^b
Triantafyllou (19) parameters				
Tumor Pattern				
Nodular	25 (41.7%)	15 (45.5%)	10 (37.0%)	0.602 ^a
Multinodular	35 (58.3%)	18 (54.5%)	17 (63.0%)	
Predominant cells				
Non luminal	51 (85.0%)	26 (78.8%)	25 (92.6%)	0.166 ^a
Luminal	9 (15.0%)	7 (21.2%)	2 (7.4%)	
Stroma				
Myxoid	57 (95.0%)	30 (90.9%)	27 (100.0%)	0.245 ^a
Chondroid	25 (41.7%)	16 (48.5%)	9 (33.3%)	0.236 ^a
Hyaline/fibrous	30 (50.0%)	17 (51.5%)	13 (48.1%)	0.795 ^a
Adipocytic	9 (15.0%)	8 (24.2%)*	1 (3.7%)	0.033 ^a
Separation between cells and stroma demarcated	51 (85.0%)	30 (90.9%)	21 (77.8%)	0.156 ^a
Crystalloids	3 (5.0%)	1 (3.0%)	2 (7.4%)	0.583 ^a
Pigmentation	4 (6.7%)	2 (6.1%)	2 (7.4%)	1.000 ^a
Vessels	24 (40.0%)	11 (33.3%)	13 (48.1%)	0.244 ^a
Nerves	7 (11.7%)	5 (15.2%)	2 (7.4%)	0.442 ^a
Average thickness of the fibrosis capsule (µm)	95.68±75.03	79.85±52.12	115.77±93.98	0.042 ^b
Dulguerov (20) parameters				
Dominant stroma				
Mucosal	2 (3.3%)	1 (3.0%)	1 (3.7%)	0.476 ^a
Myxoid	50 (83.3%)	26 (78.8%)	24 (88.9%)	
Chondroid	4 (6.7%)	2 (6.1%)	2 (7.4%)	
Fibrous	2 (3.3%)	2 (6.1%)	0 (0.0%)	
Scarce	2 (3.3%)	2 (6.1%)	0 (0.0%)	

*p<0.05; ^a, chi-square or Fisher's exact test (n, %); ^b, Mann-Whitney test (mean±SD).

Table 1. Continued

	Total	p16 (%)		p- value
		Up to 5%	>5%	
Cellular profile				
Hypocellular or stroma-rich (>50% stroma)	18 (30.0%)	7 (21.2%)	11 (40.7%)	0.252 ^a
Classic or balanced (30-50% stroma)	22 (36.7%)	14 (42.4%)	8 (29.6%)	
Hypercellular (<30% stroma)	20 (33.3%)	12 (36.4%)	8 (29.6%)	
Pseudodiploidy	3 (5.0%)	0 (0.0%)	3 (11.1%)	0.085 ^a
Satellite nodes	2 (3.3%)	1 (3.0%)	1 (3.7%)	1.000 ^a
Free surgical margins	52 (88.1%)	30 (90.9%)	22 (84.6%)	0.688 ^a
Distance from the surgical margin (cm)	0.91±0.46	0.98±0.50	0.74±0.36	0.328 ^b
Capsular integrity (%)	95.17±12.28	94.24±13.47	96.30±10.79	0.516 ^b
Minimum capsular thickness (µm)	39.83±33.81	37.12±28.15	43.15±39.98	0.542 ^b
Maximum capsular thickness (µm)	311.00±271.73	259.70±219.37	373.70±317.65	0.047 ^b
Maximum tumor size (cm)	2.70±1.19	2.68±1.11	2.74±1.31	0.955 ^b

*p<0.05; ^a, chi-square or Fisher's exact test (n, %); ^b, Mann-Whitney test (mean±SD).

ductal and myoepithelial cells showed significantly increased p16 immunostaining (p<0.001). Regarding the immunostaining profile in the stroma, we can observe that the myxoid pattern showed a higher frequency of immunostaining for p16, followed by the hyaline pattern, and the solid pattern showed the lowest expression for p16 (p<0.001) (Table 1, Figure 1).

Characterization of the sample: CxPA

Only four cases of carcinomas ex PA were raised, with ages ranging from 40-66 years, 3 in males and 1 in females, 3 in the parotid gland, and 1 in the submandibular gland.

Total resection was performed as treatment in all cases, and the smallest free margin was 0.01-0.2 cm. In none of the cases was facial nerve removal reported, and only 1 of the cases performed cervical emptying, and this was the neoplasm-free margins. The predominant pattern of the tumors was also non-luminal cells; only one case had another associated gland tumor, an adenoid cystic carcinoma (Table 2).

No cases had a perineural, vascular-lymphatic, or bony invasion. Pleomorphism was absent in one case, mild in two, and severe in another. Evident nucleoli were observed in the case that had the most cell atypia. The nucleus-cytoplasm ratio was observed in all cases, with one case having a high ratio. Mitosis figures were absent in one case, typical in one, and atypical in two. The extracapsular invasion was observed in one case, nuclear pleomorphism in three of the four cases, atypical mitoses in two, hemorrhage and necrosis in one case, which coincided with the case with the highest cell atypia and located in the submandibular gland (Table 2).

Regarding the immunostaining profile for p16, none of the cases showed immunopositivity in periductal cells, the three parotid cases showed immunostaining in ductal cells, and one parotid case and the submandibular case showed mild immunostaining for myoepithelial cells. In addition, myxoid stroma was seen in 2 cases, and the immunostaining profile ranged from 1-20% of labeled cells showing a mean of 7.00±8.83% (Table 2, Figure

2). There was no significant difference between p16 immunostaining of PA and CxPA (p=0.537).

Influence of immunostaining for p16 on the clinicopathological profile of PAs

Regarding the number of cells marked for p16 with the clinicopathological patterns, no pattern showed a significant association; however, those who did not have an adipocytic stromal profile in the histological feature of Triantafyllou (19) showed lower p16 expression, suggesting that this stromal profile is inversely associated with p16 protein expression (p=0.033). Additionally, cases with higher p16 expression had significantly higher mean fibrous capsule thickness than those with low expression (p=0.042), while p16 positive cases had higher mean maximum capsular thickness than p16 negative cases (p=0.047) (Table 3).

Regarding the influence of cell profile on p16 immunostaining in PAs, periductal and ductal cells did not influence the amount of total labeled cells. However, myoepithelial cells were directly associated with increased p16 expression (p<0.001) (Table 4).

Cases with myxoid stroma, hyaline stroma, and chondroid stroma were also directly associated with increased p16 (p<0.001), and myoepithelial cells (p<0.001) present precisely in these stromal (Table 4).

Discussion

The study of clinicopathological characteristics of tumors, even benign ones, is essential to predict their biological behavior and, consequently, prognosis. PA is a benign tumor, but it may sometimes have aggressive characteristics that need to be associated with its cellular and biological profile. The present sample showed a predilection for females, close to the proportion reported in other studies, and a wide age range similar to that previously described (Almeslet, 2020; Tarakji et al., 2013; Dardick et al., 1982; Sharma et al., 2018). The most common location of PA was in the parotid gland,

Table 2. Clinicopathological Characterization and Immunostaining for p16 in Cx PA

Cases	CxPA			
	1	2	3	4
Morais (21) and Toluie (23) parameters				
Predominant Pattern				
Luminal	N	Y	N	N
Non-luminal	Y	N	Y	N
Other associated gland tumor	N	Y*	N	N
Perineural invasion (21, 23)	N	N	N	N
Angiolymphatic invasion (21, 23)	N	N	N	N
Bone invasion (21, 23)	N	N	N	N
Pleomorphism (A/L/M/S)	Mild	Mild	Absent	Severe
Nucleoli	N	N	N	Y
Nucleus-cytoplasm relationship (21, 23)	Y	Y	Y	Y ²
Mitosis figures	Typical	Atypical	Absent	Atypical
Extracapsular invasion	N	N	Y	N
Nuclear pleomorphism	Y	Y	N	Y
Atypical mitoses	N	Y	N	Y
Hemorrhage	N	N	N	Y
Necrosis	N	N	N	Y
Antony (22) and Toluie (23) parameters				
Age	50	43	40	66
Sex	M	F	M	M
Tumor site	Parotid	Parotid	Parotid	Submandibular
Resection	Total	Total	Total	Total
Smallest free margin (mm)	0.2 cm	0.1 cm	0.01 cm	0.1 cm
Facial nerve removal	Not reported	Not reported	Not reported	Not reported
Cervical Emptying (22,23)	N	N	N	Yes
Nodal metastasis	N	N	N	N
p16				
Cells				
Periductal	-	-	-	-
Ductal	++	+	+++	-
Myoepithelial	+	-	+	+
Stroma				
Myxoid	-	-	+	+
Hyaline	-	-	NA	NA
Chondroid	-	NA	-	NA
Solid	-	-	+	-
Percentage of labeled cells	5%	1%	20%	2%

*Yes, adenoid cystic carcinoma; Y, Yes; Y², high nucleus-cytoplasm ratio; N, No; NA, not assessed.

followed by the submandibular gland, in line with other studies, such as that of Handa et al., (2009) whose series showed 80% of cases in the parotid gland and 12% in the submandibular gland. Moreover, multifocal tumors seem equally rare in our sample (Bartkowiak et al., 2022).

Regarding microscopic features, we observed a higher frequency of squamous metaplasia than the approximately 25% described in the literature (Dardick et al., 1982). According to Sharma et al., (2018), squamous cell foci are an integral feature of PA. Still, extensive squamous metaplasia is uncommon and may be misinterpreted as

squamous cell carcinoma of salivary glands, completely changing the therapeutic management. In the present study, squamous metaplasia was the most prevalent, but when present, it was not extensive, reaching less than half of the tumor in 38.3% of the cases. Only five cases presented keratin pearls (8.3%).

The main cells constituting the epithelial region of the PA were non-luminal cells, present in 85.0% of cases (n=51). The stromal areas in all cases analyzed by Lee et al., (2000) were composed predominantly of non-luminal cells. In 2009, Handa et al., (2009) also evidenced that

Table 3. Immunohistochemical Characterization of PAs

	Cells			p- Value	Stroma				p- Value
	Periductal	Ductal	Myoepithelial		Myxoid	Hyaline	Chondroid	Solid	
p16									
-	48 (80.0%)*	15 (25.0%)	15 (25.0%)	<0.001	19 (32.2%)	21 (65.6%)	13 (54.2%)	50 (87.7%)*	<0.001
+	12 (20.0%)	30 (50.0%)*	25 (41.7%)*		20 (33.9%)*	8 (25.0%)*	7 (29.2%)*	6 (10.5%)	
++	0 (0.0%)	13 (21.7%)*	14 (23.3%)*		15 (25.4%)*	3 (9.4%)	4 (16.7%)	1 (1.8%)	
+++	0 (0.0%)	2 (3.3%)*	6 (10.0%)*		5 (8.5%)	0 (0.0%)	0 (0.0%)	0 (0.0%)	

*p<0.05, chi-square, or Fisher's exact test (n, %). The mean and median percentage of immunoeexpression for p16 were 11.35±13.93% and 5%, respectively, ranging from 0-50%.

Table 4. Influence of Cell Profile on p16 Immunostaining in PAs

	p16 (%)		p-Value
	Up to 5%	>5%	
Periductal cells			
-	27 (81.8%)	21 (77.8%)	0.697
+	6 (18.2%)	6 (22.2%)	
++	0 (0.0%)	0 (0.0%)	
+++	0 (0.0%)	0 (0.0%)	
Ductal cells			
-	10 (30.3%)	5 (18.5%)	0.159
+	14 (42.4%)	16 (59.3%)	
++	9 (27.3%)	4 (14.8%)	
+++	0 (0.0%)	2 (7.4%)	
Myoepithelial cells			
-	14 (42.4%)*	1 (3.7%)	<0.001
+	16 (48.5%)*	9 (33.3%)	
++	2 (6.1%)	12 (44.4%)*	
+++	1 (3.0%)	5 (18.5%)*	
Myxoid Stroma			
-	17 (53.1%)*	2 (7.4%)	<0.001
+	11 (34.4%)	9 (33.3%)	
++	4 (12.5%)	11 (40.7%)*	
+++	0 (0.0%)	5 (18.5%)*	
Hyaline Stroma			
-	17 (85.0%)*	4 (33.3%)	0.006
+	3 (15.0%)	5 (41.7%)*	
++	0 (0.0%)	3 (25.0%)*	
+++	0 (0.0%)	0 (0.0%)	
Chondroid Stroma			
-	11 (68.8%)*	2 (25.0%)	0.007
+	5 (31.3%)*	2 (25.0%)	
++	0 (0.0%)	4 (50.0%)*	
+++	0 (0.0%)	0 (0.0%)	
Solid Stroma			
-	29 (90.6%)	21 (84.0%)	0.486
+	3 (9.4%)	3 (12.0%)	
++	0 (0.0%)	1 (4.0%)	
+++	0 (0.0%)	0 (0.0%)	

*p<0.05, chi-square, or Fisher's exact test (n, %).

myxoid stroma was present in most cases, and variations in the appearance of the stromal component as chondroid, hyaline, fibrous, and bony were also observed in histological sections. The present study revealed that the dominant stroma was myxoid, followed by chondroid and mucous. The maximum mean tumor size was 2.70±1.19 centimeters, values very similar to that described by Bartkowiak et al., (2022) (3.0±1.78 cm).

Regarding the expression of p16 protein in PAs, the immunolabeling profile was quite variable since they sometimes marked ductal, periductal, and sometimes myoepithelial cells. In the present study, we observed negative immunostaining for p16 in most periductal cells and positive immunostaining for p16 in myoepithelial cells, corroborating the study by Jour et al., (2013). Furthermore, they described that PA expressed p16INK4A, especially in epithelial and myoepithelial cells.

According to Patel et al., (2007) PA and CxAP expressed p16INK4A in the neoplastic epithelial and myoepithelial components. Furthermore, they evidenced a higher expression of p16 in the benign epithelial component than a malignant component of CxPA, hypothesizing a “protective” effect for p16 against the progression of PA to carcinoma ex-adenoma pleomorphic. Corroborating with the present study's findings, the immunolabeling profile of p16 in CxPA was lower than in PA.

Regarding the clinicopathological characterization and p16 immunostaining of the four ex-PA carcinomas analyzed in this study, it was evidenced that most cases were male, with ages ranging from 40-66 years. In the study by Hu et al., (2011) from the 50 CxAP analyzed, most cases were also male (n=36), with the age range also slightly higher than that of PA, ranging from 34 to 78 years. The cases of CxPA were mainly located in the parotid gland, which corroborates with the study of Okano et al., (2020) and the treatment mainly based on wide surgical resection (Gupta et al., 2019), and may or may not be indicated cervical emptying if nodal metastasis is suspected (Antony et al., 2012). In the present study, in only one of the cases, it was necessary to perform cervical emptying, the margins free of neoplasia.

Regarding microscopic features, the predominant pattern of the tumors was non-luminal cells. Still, according to the study by Demasi et al., (2009) the epithelial (luminal) component formed 75% of all CxAP cases (n=16). CxPA also presents severe nuclear pleomorphism with prominent nucleoli, frequent and/

or atypical mitotic figures, and vascular, capsular, and perineural invasion and hemorrhagic and necrotic foci (Di Palma, 2013; Khana et al., 2019). In the present study, only one case (25%) demonstrated a high degree of cellular atypia, being precisely the case that presented low p16 expression since it has been suggested that p16 immunostaining in carcinomas ex PAs is often downregulated.

The role of the p16 protein is to inhibit cyclin-dependent kinase 4 (CDK4), preventing the phosphorylation of pRb and blocking cell cycle progression from G1 to S phase (Zhang et al., 1999). In head and neck squamous cell carcinoma, it is common to have a loss of p16 expression that may be related to a worse prognosis of this tumor (Namazie et al., 2002; Worsham et al., 2006). According to Stephen et al., (2013) protein immunostaining is an important prognostic indicator in cases of oropharyngeal squamous cell carcinoma since patients positive for p16 had an improved overall survival for all sites analyzed in the study.

Thus, this study demonstrated that despite the wide variation in microscopic features of PA, its biological behavior is quite predictable and that loss of p16 immunostaining seems to be related to more aggressive microscopic features and possibly to evolution to CxPA. Perhaps the major limitation of this study is the small sample size of carcinomas ex PA due to the tumor's rarity. Still, the extensive histological review directs to an essential role in the control of cellular aggressiveness of these salivary gland tumors by p16 immunostaining.

The microscopic features of the PA and CxPA of the present sample are similar to those evaluated in the literature. The loss of expression for p16 in parts of its components seems to be related to microscopic features of aggressiveness. Cohort studies are needed to evaluate whether this marker can be a prognostic marker for these two tumors

Author Contribution Statement

Fabricio Bitu Sousa and Paulo Goberlanio Barros Silva design the study, they read and approve the final version of article. Kecynara Costa Barbosa and Iana Aragao Magalhaes performed histologic analysis of PA, they read and approve the final version of article. Gabriella Alves Juliao Costa and Osias Vieira Oliveira Filho performed histologic analysis of CxPA, they read and approve the final version of article. Jose Erialdo da Silva Junior performed p16 immunohistochemical analysis of PA and CxPA, he read and approve the final version of article. Lucio Flavio Gonzaga Silva and Sergio Ferreira Juaçaba revised clinic data and rescue paraffin blocks and medical records, They read and approve the final version of article.

Acknowledgements

We would like to thank the Hospital Haroldo Juaçaba (HHJ) – Cancer Institute of Ceará for the contributions to this research, for providing the infrastructure for the execution of this study.

Funding Information

Cearense Research Support Foundation (FUNCAP) in the form of a scientific initiation scholarship.

Data Availability Statement

Data sharing not applicable to this article as no datasets were generated or analyzed during the current study.

Fundin Statement

This study was partially funded by the Cearense Foundation for Scientific and Technological

Development Support

(FUNCAP – Fundação Cearense de Apoio ao Desenvolvimento Científico e Tecnológico) through a scientific initiation grant.

Scientific Body Approval

This study was approved by the examining board of the Scientific Initiation Program of the Ceará Cancer Institute. This study was not part of a thesis or dissertation.

Ethic Approval

This research was submitted to the Research Ethics Committee of the HHJ/ICC, observing the norms that regulate research with human beings, of the Brazilian National Health Council under resolution 466/12. The opinion number was 2.251.564.

Conflict Of Interest

The authors have no conflicts of interest.

References

- Ahmedi JR, Ahmedi E, Perjuci F, et al (2017). Pleomorphic Adenoma of Minor Salivary Glands in Child. *Med Arch*, **71**, 360-3.
- Almeslet AS (2020). Pleomorphic Adenoma: A Systematic Review. *Int J Clin Pediatr Dent*, **13**, 284-7.
- Andreasen S, Therkildsen MH, Bjørndal K, Homøe O (2016). Pleomorphic adenoma of the parotid gland 1985-2010: A Danish nationwide study of incidence, recurrence rate, and malignant transformation. *Head Neck*, **38**, eE1364-9.
- Antony J, Gopalan V, Smith RA, Lam AKY (2012). Carcinoma ex pleomorphic adenoma: a comprehensive review of clinical, pathological and molecular data. *Head Neck Pathol*, **6**, 1-9.
- Bartkowiak E, Piwowarczyk K, Bodnar M, et al (2022). Expression of p16Ink4a protein in pleomorphic adenoma and carcinoma ex pleomorphic adenoma proves diversity of tumour biology and predicts clinical course. *J Clin Pathol*, **75**, 605-11.
- Batsakis JG, Kraemer B, Sciubba JJ (1983). The pathology of head and neck tumors: The myoepithelial cell and its participation in salivary gland neoplasia, part 17. *Head Neck Surg*, **5**, 222-33.
- Choi JS, Cho BH, Kim HJ, Kim YM, Jang JH (2019). Identification of new genes of pleomorphic adenoma. *Medicine (Baltimore)*, **98**, e18468.
- Dardick I, van Nostrand AW, Phillips MJ (1982). Histogenesis of salivary gland pleomorphic adenoma (mixed tumor) with an evaluation of the role of the myoepithelial cell. *Hum Pathol*, **13**, 62-75.
- Dardick I, van Nostrand AW (1985). Myoepithelial cells in *Asian Pacific Journal of Cancer Prevention*, Vol 24 **3823**

- salivary gland tumors - revisited. *Head Neck Surg*, **7**, 395-408.
- Demasi APD, Furuse C, Soares AB, et al (2009). Peroxiredoxin I, platelet-derived growth factor A, and platelet-derived growth factor receptor α are overexpressed in carcinoma ex pleomorphic adenoma: association with malignant transformation. *Hum Pathol*, **40**, 390-7.
- Di Palma S (2013). Carcinoma ex pleomorphic adenoma, with particular emphasis on early lesions. *Head Neck Pathol*, **1**, s68-76.
- Dulguerov P, Todic J, Pusztaszeri M, Alotaibi NH (2017). Why do parotid pleomorphic adenomas recur? A systematic review of pathological and surgical variables. *Front Surg*, **4**, 26.
- Erdem MA, Cankaya AB, Güven G, Olgaç V, Kasapoğlu C (2011). Pleomorphic adenoma of the palate. *J Craniofac Surg*, **22**, 1131-4.
- Gupta A, Koochakzadeh S, Neskey DM, Nguyen SA, Lentsch EJ (2019). Carcinoma ex pleomorphic adenoma: a review of incidence, demographics, risk factors, and survival. *Am J Otolaryngol*, **40**, 102279.
- Handa U, Dhingra N, Chopra R, Mohan H (2009). Pleomorphic adenoma: Cytologic variations and potential diagnostic pitfalls. *Diagn Cytopathol*, **37**, 11-5.
- Hellquist H, Paiva-Correia A, Poorten VV, et al (2019). Analysis of the clinical relevance of histological classification of benign epithelial salivary gland tumours. *Adv Ther*, **36**, 1950-74.
- Hu YH, Zhang CY, Tian Z, et al (2011). Aberrant protein expression and promoter methylation of p16 gene are correlated with malignant transformation of salivary pleomorphic adenoma. *Arch Pathol Lab Med*, **135**, 882-9.
- Jain S, Hasan S, Vyas N, Shah N, Dalal S (2015). Pleomorphic adenoma of the parotid gland: Report of a case with review of literature. *Ethiop J Health Sci*, **25**, 189-94.
- Jour G, West K, Ghali V, et al (2013). Differential Expression of p16INK4A and Cyclin D1 in Benign and Malignant Salivary Gland Tumors: A Study of 44 Cases. *Head Neck Pathol*, **7**, 224-31.
- Khanna D, Chaubal T, Bapat R, et al (2019). Carcinoma ex pleomorphic adenoma: a case report and review of literature. *Afr Health Sci*, **19**, 3253-63.
- Lee PS, Sabbath-Solitare M, Redondo TC, Ongcapin EH (2000). Molecular evidence that the stromal and epithelial cells in pleomorphic adenomas of salivary gland arise from the same origin: clonal analysis using Human Androgen Receptor Gene (HUMARA) Assay. *Hum Pathol*, **31**, 498-503.
- Morais EF, Pinheiro JC, Sena DAC, et al (2019). Extracapsular invasion: A potential prognostic marker for Carcinoma ex pleomorphic adenoma of the salivary glands? A Systematic Review. *J Oral Pathol Med*, **48**, 433-40.
- Namazie A, Alavi S, Olopade OI, et al (2002). Cyclin D1 amplification and p16 (MTS1/CDK4I) deletion correlate with poor prognosis in head and neck tumors. *Laryngoscope*, **112**, 472-81.
- Okano K, Ishida M, Sandoh K, et al (2020). Cytological features of carcinoma ex pleomorphic adenoma of the salivary glands: A diagnostic challenge. *Diagn Cytopathol*, **48**, 149-53.
- Patel RA, Rose B, Bawdon H, et al (2007). Cyclin D1 and p16 expression in pleomorphic adenoma and carcinoma ex pleomorphic adenoma of the parotid gland. *Histopathology*, **51**, 691-6.
- Reinheimer A, Vieira DS, Cordeiro MM, Rivero ER (2019). Retrospective study of 124 cases of salivary gland tumors and literature review. *J Clin Exp Dent*, **11**, e1025-32.
- Romagosa C, Simonetti S, López-Vicente L, et al (2011). p16Ink4a overexpression in cancer: a tumor suppressor gene associated with senescence and high-grade tumors. *Oncogene*, **30**, 2087-97.
- Seok J, Hyun SJ, Jeong WJ, et al (2019). The Difference in the Clinical Features Between Carcinoma ex Pleomorphic Adenoma and Pleomorphic Adenoma. *Ear Nose Throat J*, **98**, 504-9.
- Sergi B, Limongelli A, Scarano E, Fetoni AR, Paludetti G (2008). Giant deep lobe parotid gland pleomorphic adenoma involving the parapharyngeal space. report of three cases and review of the diagnostic and therapeutic approaches. *Acta Otorhinolaryngol Ital*, **28**, 261-5.
- Serrano M, Hannon GJ, Beach D (1993). A new regulatory motif in cell-cycle control causing specific inhibition of cyclin D/CDK4. *Nature*, **366**, 704-7.
- Sharma S, Mehendiratta M, Chaudhary N, et al (2018). Squamous metaplasia in pleomorphic adenoma: a diagnostic and prognostic enigma. *J Pathol Transl Med*, **52**, 411-5.
- Stephen JK, Divine G, Chen KM, et al (2013). Significance of p16 in site-specific HPV positive and HPV negative head and neck squamous cell carcinoma. *Cancer Clin Oncol*, **2**, 51-61.
- Tarakji B, Altamimi MA, Baroudi K, Nassain MZ, Alenzi FQ (2013). Immunohistochemical expression of p16 in carcinoma ex-pleomorphic adenoma (undifferentiated and adenocarcinoma types). *J Clin Diagn Res*, **7**, 3054-6.
- Thompson L (2006). World Health Organization classification of tumours: pathology and genetics of head and neck tumours. *Ear Nose Throat J*, **85**, 74.
- Toluie S, Thompson LDR (2012). Sinonasal tract adenoid cystic carcinoma ex-pleomorphic adenoma: a clinicopathologic and immunophenotypic study of 9 cases combined with a comprehensive review of the literature. *Head Neck Pathol*, **6**, 409-21.
- Triantafyllou A, Thompson LDR, Devaney KO, et al (2015). Functional histology of salivary gland pleomorphic adenoma: an appraisal. *Head Neck Pathol*, **9**, 387-404.
- Vageli D, Sourvinos G, Ioannou M, Koukoulis GK, Spandidos DA (2007). High-risk human papillomavirus (HPV) in parotid lesions. *Int J Biol Markers*, **22**, 239-44.
- Worsham MJ, Chen KM, Tiwari N, et al (2006). Fine-mapping loss of gene architecture at the CDKN2B (p15INK4b), CDKN2A (p14ARF, p16INK4a), and MTAP genes in head and neck squamous cell carcinoma. *Arch Otolaryngol Head Neck Surg*, **132**, 409-15.
- Zhang HS, Postigo AA, Dean DC (1999). Active transcriptional repression by the Rb-E2F complex mediates G1 arrest triggered by p16INK4a, TGF β , and contact inhibition. *Cell*, **97**, 53-61.



This work is licensed under a Creative Commons Attribution-Non Commercial 4.0 International License.